

Polarimetric Radar-Based Estimates of Spatial Variability in Characteristic Sizes of Raindrops in Stratiform Rainfall

SERGEY Y. MATROSOV

Cooperative Institute for Research in Environmental Sciences, University of Colorado, and NOAA/Earth System Research Laboratory, Boulder, Colorado

(Manuscript received 11 March 2011, in final form 27 June 2011)

ABSTRACT

Polarimetric X-band radar measurements of differential reflectivity Z_{DR} in stratiform rainfall were used for retrieving mean mass-weighted raindrop diameters D_m and estimating their spatial variability δD_m at different scales. The Z_{DR} data were calibrated and corrected for differential attenuation. The results revealed greater variability in D_m for larger spatial scales. Mean values of δD_m were respectively around 0.32–0.34, 0.28–0.30, and 0.24–0.26 mm at scales of 20, 10, and 4.5 km, which are representative of footprints of various spaceborne sensors. For a given spatial scale, δD_m decreases when the mean value of D_m increases. At the 20-km scale the decreasing trend exhibits a factor-of-1.7 decrease of δD_m when the average D_m changes from 1 to 2 mm. Estimation data suggest that this trend diminishes as the spatial scale decreases. Measurement noise and other uncertainties preclude accurate estimations of D_m variability at smaller spatial scales because for many data points estimated variability values are equal to or less than the expected retrieval errors. Even though they are important for retrievals of absolute values of D_m , the details of the drop shape–size relation did not significantly affect estimates of size spatial variability. The polarization cross coupling in simultaneous transmission–simultaneous receiving measurement mode presents another limiting factor for accurate estimations of D_m . This factor, however, was not too severe in estimations of the size variability. There are indications that tuning the differential attenuation correction scheme might balance off some possible cross-coupling Z_{DR} bias if differential phase accumulation is less than approximately 40° .

1. Introduction

Dual-polarization radars have been used for retrievals of raindrop size distributions (DSDs) for a number of years (e.g., Chandrasekar et al. 2008 and references therein). A three-parameter gamma function and its different modifications (e.g., the normalized gamma function) are usually used for theoretical representations of DSDs in rainfall (e.g., Ulbrich 1983; Willis 1984). In the conventional form of the gamma function, drop number concentrations $N(D)$ are expressed as $N(D) = N_0 D^\mu \exp[-(3.67 + \mu)D/D_0]$ as a function of drop size D , where three parameters defining the gamma function are the N_0 parameter, the shape parameter μ , and the median volume drop size D_0 . Because raindrops are generally nonspherical, the drop size D is usually understood as the diameter of the equal-volume sphere.

Sometimes the characteristic drop size of a DSD is expressed in terms of the mass-weighted mean drop diameter D_m . For untruncated gamma distributions, this characteristic size is closely related to D_0 as

$$D_m = D_0(4 + \mu)(3.67 + \mu)^{-1}. \quad (1)$$

Usually D_m differs from D_0 by not more than 10%–12%, because μ is generally greater than -1 [see, for example, experimental data from Zhang et al. (2003)]. In some applications, the exponential slope parameter $\Lambda = (3.67 + \mu)/D_0$ is used as a size parameter instead of the characteristic drop size.

Polarimetric precipitation radars typically operate in the horizontal–vertical (HV) polarization basis, and their main parameters (in addition to the reflectivity factor Z_e , hereinafter referred to as just reflectivity), which are used for rainfall DSD retrievals, are differential reflectivity (Z_{DR}) and the specific differential propagation phase shift (K_{DP}), which is estimated as a range derivative of the filtered differential phase shift

Corresponding author address: Sergey Y. Matrosov, R/PSD2, 325 Broadway, Boulder, CO 80305.
E-mail: sergey.matrosov@noaa.gov

Φ_{DP} measurements. The K_{DP} values are often very noisy and are of limited use for DSD retrievals in rainfalls that result in reflectivities of less than approximately 29–30 dBZ for X-band (~ 10 GHz) observations and in rainfalls with reflectivities of less than about 34–35 dBZ for S-band (~ 3 GHz) observations (Matrosov et al. 2006).

Differential reflectivity Z_{DR} measurements, which represent the logarithmic difference between horizontal and vertical polarization reflectivities, are also somewhat noisy. Unlike for K_{DP} , however, these measurements are available also for lighter rainfall. It has been shown (e.g., Seliga and Bringi 1976) that Z_{DR} measurements can be used for direct estimates of raindrop characteristic sizes D_0 (or D_m). Relations between differential reflectivity and characteristic drop sizes are determined by the degree of drop nonsphericity, which is size dependent. Retrievals (of raindrop characteristic sizes) that are based on Z_{DR} have been performed in many studies (e.g., Bringi and Chandrasekar 2001). Although estimates of all gamma-function DSD parameters can be available from polarimetric radar measurements (except for lighter rains, which do not exhibit pronounced polarization signatures), Z_{DR} -based retrievals of characteristic drop sizes are, probably, the most straightforward.

The availability of drop size information from radar polarimetric measurements can be useful in many practical applications ranging from rain microphysical studies to developments of space-based algorithms for rainfall retrievals. In the latter case, the horizontal spatial variability of characteristic drop sizes within a footprint of a spaceborne remote sensor is an important factor influencing retrieval uncertainties. This variability is expected to be different at different spatial scales, and therefore high-resolution polarimetric radar retrievals can provide valuable information for algorithm assessments.

The main objectives of this study were 1) the estimation of uncertainties of X-band radar Z_{DR} measurements (including those due to “polarization cross coupling”), 2) the assessment of errors of inferring raindrop characteristic sizes from Z_{DR} data, and 3) the evaluation of variability in these sizes at different spatial scales representing fields of view of various satellite sensors. The data for this study were collected by the National Oceanic and Atmospheric Administration (NOAA) X-band polarimetric radar for hydrometeorological research (HYDROX) during its deployment at the Hydrometeorological Test Bed (HMT) field experiment. The specificity of the HYDROX scanning strategy and maximum range limitations allowed estimations of characteristic drop size variability at spatial scales up to 20 km. Note that the spatial scales in the interval from about 4.5

to 20 km approximately correspond to footprints of the Tropical Rainfall Measuring Mission (TRMM) precipitation radar (~ 4.5 km) and higher-frequency (20–85 GHz) channels of the TRMM Microwave Imager (~ 5 –20 km).

2. Observational and retrieval data

During the HMT field project of the 2005/06 season (HMT-06), the HYDROX radar was deployed near Auburn, California. This radar operates at a wavelength of 3.2 cm and has full scanning capability. Its main technical parameters are given by Matrosov et al. (2005). The simultaneous transmission–simultaneous receiving (STSR) of horizontally and vertically polarized signals is used with the HYDROX radar. This measurement scheme is currently employed by many research radars, and it is being implemented with the polarimetric upgrade of the National Weather Service radars in the United States (Doviak et al. 2000).

The routine scanning procedure employed with the radar included 3° elevation plan position indicator (PPI) scans in a 90° quadrant oriented toward the American River basin (ARB). Lower-elevation measurements were not possible because of terrain blockage. The observed reflectivity and Z_{DR} measurements were corrected for the effects of attenuation and differential attenuation using differential phase-shift measurements as described by Matrosov (2010). The along-beam resolution of the HYDROX measurements was 150 m, and the maximum radar range during the HMT-06 deployment was 38 km. The radar beamwidth of about 0.9° provided a cross-beam resolution of approximately 600 m at the maximum range.

The observed wintertime rainfall was largely of the stratiform type with a clearly defined radar bright band caused by the reflectivity enhancements in the layer of melting hydrometeors. The height of the melting layer during observations was reaching about 1.5–2.3 km above the ground at the radar location for the warmest events observed in December of 2005 and early January of 2006. These events were the main interest for this study because the variability of radar-based estimates of characteristic drop sizes could be assessed at different spatial scales. The precipitation events observed later in the season were generally colder, and brightband features were routinely observed at the ranges of about 5–15 km from the radar (Matrosov et al. 2007) so that the HYDROX radar coverage area was mostly filled with returns from snow and melting-layer regions. Rain rates during the warmer events were typically in a range between 0.5 and 12 mm h⁻¹ (as inferred from radar and gauge/disdrometer measurements).

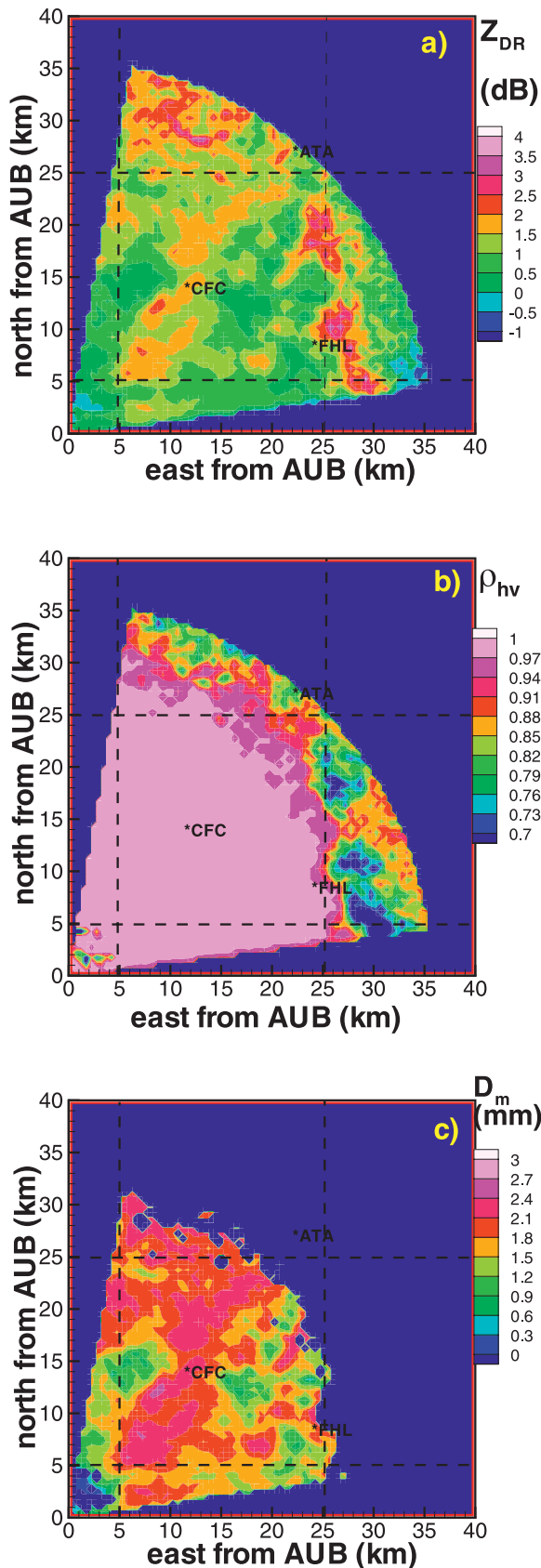


Figure 1a shows an example of HYDROX Z_{DR} data, which were corrected for the differential attenuation effects in rainfall. The HYDROX radar data were gridded at a 500 m by 500 m resolution, which was dictated by rainfall rate and accumulation estimate comparisons with nonpolarimetric radars operating in the ARB area. The original 150-m-range-resolution HYDROX data corrected for differential attenuation within each grid cell were averaged (in the linear scale) to provide 500-m Cartesian grid data. The three-letter abbreviations for the radar location (i.e., AUB) and for locations of the rain gauges (CFC, ATA, and FHL) are used in this figure. The presented PPI scan was conducted during one of the priority HMT-06 events observed during 30–31 December 2005.

The measurement data for the copolar correlation coefficient ρ_{hv} , which correspond to the Z_{DR} values in Fig. 1a, are shown in Fig. 1b. The use of ρ_{hv} allows differentiating among the rain, melting hydrometeors, and snow regions in stratiform precipitation. Because ρ_{hv} is generally greater than about 0.96–0.97 in rain for strong echoes, it can be concluded that the arc of increased differential reflectivity in Fig. 1a observed at distances greater than about 25–27 km is a result of backscatter from the melting layer. The copolar correlation coefficient also helps to identify the ground clutter (see in Fig. 1b examples of ground clutter manifested by small areas of low ρ_{hv} values observed at shorter distances under 5 km from the AUB site).

The retrievals of the mass-weighted mean drop diameter D_m are shown in Fig. 1c. These retrievals are based on HYDROX differential reflectivity data. The D_m – Z_{DR} relation used for the conversion is

$$D_m \text{ (mm)} = 1.8Z_{DR}^{0.4} \text{ (dB)}. \quad (2)$$

This relation was obtained using the experimental DSDs measured by a Joss–Waldvogel impact disdrometer located at the CFC site during the HMT-06 field deployment. The disdrometer drop count measurements were corrected for the “dead time” effects using a procedure suggested by Sheppard and Joe (1994). The general robustness of experimental DSD from the disdrometer was supported by good agreement between rainfall accumulations calculated using these DSDs and results obtained from standard meteorological rain gauges (Matrosov 2010).

FIG. 1. Examples of the HYDROX estimates of (a) Z_{DR} , (b) ρ_{hv} , and (c) D_m during routine PPI scans performed at 1453 UTC 30 Dec 2005.

The coefficients in the D_m - Z_{DR} relation depend on drop aspect ratios expressed as a function of drop size. The raindrop shapes usually are modeled by oblate spheroids. Drops that are smaller than about 0.5 mm in diameter are practically spherical, and they do not produce any reliably measurable polarization effects. Mean aspect ratios of larger drops monotonically decrease as drop sizes increase, reaching a value of about 0.7 for a 5-mm drop diameter. Recent experimental observations of drop shapes obtained from wind-tunnel measurements and from 2D video disdrometer measurements (Thurai et al. 2009) indicate that mean aspect ratios of falling drops generally agree with the model results of Beard and Chuang (1987). These results were also satisfactorily described by a polynomial approximation fit (Brandes et al. 2005) of earlier experimental datasets from different authors. Although these datasets had been collected using different techniques (and with different degrees of accuracy), in a mean sense they generally agreed with the later more-precise experimental data (e.g., from Thurai et al. 2009).

For the HMT-06 experimental DSDs, the coefficients in Eq. (2) were obtained using the T-matrix calculation method (Barber and Yeh 1975) for computing Z_{DR} and the polynomial approximation for drop aspect ratio. The D_m values were calculated as a ratio of the fourth and the third moments of observed DSDs. It was assumed during calculations that the radar elevation angle is 3° (as in observations), the mean drop canting angle in the radar polarization plane is zero, and the canting angle distribution is Gaussian with an 8° standard deviation. Such assumptions about raindrop orientations are generally in line with recent experimental observations by Huang et al. (2008). The Brandes et al. (2005) polynomial approximation for the drop aspect ratio–size relation was used.

HYDROX radar differential reflectivity measurements were calibrated using vertical beam observations in light drizzle-like rain in low wind conditions. Because of the azimuthal symmetry of targets, such observations should result in $Z_{DR} \approx 0$ dB (Bringi and Chandrasekar 2001), and therefore vertical beam data can be used to remove any initial Z_{DR} measurement bias. In addition to removing the initial bias, the vertical beam observations can be used for assessing a Z_{DR} measurement uncertainty from estimates of the standard deviation of differential reflectivity data.

Figure 2a shows the results of individual Z_{DR} measurements with the antenna pointing at zenith after the mean bias was removed (note that differential attenuation effects on vertical measurements of Z_{DR} are absent). The data are presented as a function of the received power at the antenna terminals P_0 . The linear range of

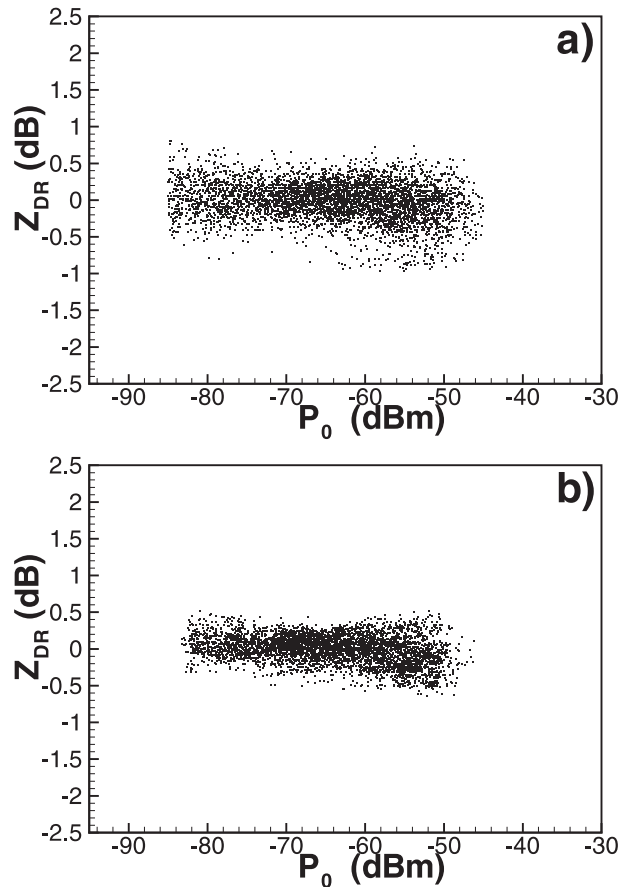


FIG. 2. Scatterplots of Z_{DR} measurements with vertically pointing radar beam: (a) individual measurement results and (b) five-point running averages.

the HYDROX radar receivers during the HMT-06 deployment was for power values in a range between about -90 and -45 dBm. Rainfall with $Z_e > 16$ dBZ was considered in this study. The analyzed data generally corresponded to $P_0 > -85$ dBm, which was at least 15 dB higher than the radar-receiver noise floor. The standard deviation of the data points in Fig. 2a is 0.26 dB. There is some indication that the Z_{DR} biases are slightly different at the low and high power ends in Fig. 2 (which may be due to a not-perfect match of the horizontal and vertical polarization receiver gains in the whole linear dynamic range), but the corresponding differences are generally smaller than 0.1 dB and were neglected. It is further assumed that 0.26 is a measure of the uncertainty of individual differential reflectivity measurements.

Averaging several data points reduces data scatter and thus can reduce measurement uncertainties for gridded values. Figure 2b shows the data scatter of vertical beam measurements when a five-point running-window

averaging was used for the individual Z_{DR} measurements presented in Fig. 2a. This averaging resulted in a decrease of the standard deviation value to about 0.2 dB. It is further assumed that this value is representative of the uncertainty of the gridded Z_{DR} data (like those in Fig. 1a) representing measurement noise. This assumption could be somewhat conservative because usually more than five individual points are used to represent one grid point (except for the longest ranges). To remove data, which are likely to be very noisy, D_m retrievals were not attempted when mean values of Z_{DR} corrected for differential attenuation in the gridded resolution points were less than a threshold of 0.2 dB. This threshold corresponds to the D_m value of about 0.9 mm. Some small bias resulting from such thresholding is not out of the question, but it was neglected here. The antenna sidelobes of the HYDROX data are at the level from about -23 to -25 dB for the 3° elevation angle. It was further assumed that in stratiform rainfall contamination of Z_{DR} data through the sidelobes can be neglected.

3. Variability of D_m at different spatial scales

a. Assessing the variability of mass-weighted drop sizes

Polarimetric radar-based retrievals of the mass-weighted mean drop diameter D_m can be used for estimation of the variability of the characteristic drop size at different scales. Given the relatively small range of the HYDROX radar, the largest horizontal scale at which this variability can be effectively estimated is about 20 km, which is representative of a resolution of spaceborne microwave radiometers. The largest square with a 20-km side, which is entirely covered by the HYDROX measurements, is outlined in Fig. 1 by dashed lines. It is centered at a point located at a distance of 21.2 km in a northeast direction (15 km north and 15 km east) from the radar site at Auburn. This square excludes the small area of ground clutter near the radar and contains 1600 grid-resolution cells. It should be mentioned that this square is slightly distorted relative to the ideal geometrical figure. This is due to the slanted geometry of radar observations. This distortion, however, is somewhat small and is neglected.

The D_m variability was estimated as the standard deviation of retrieved mass-weighted mean drop diameters (δD_m) in the square mentioned above. To assess how the drop characteristic size variability changes with the scale, the δD_m estimations were also performed for smaller-size squares. For consistency of estimates, the centers of these squares were coincident with the 20-km

square. For a given scan at each resolution scale, the estimates of δD_m were performed if at least 90% of the area for a given square was filled with rain ($\rho_{hv} \geq 0.96$). The maximum number of samples was 1600, 400, and 81 for the scales of 20, 10, and 4.5 km, correspondingly. The example shown in Fig. 1c for the 20-km square fits this requirement because Z_{DR} -based D_m retrievals are not available only in a small area at longer distances. Returns from the regions with $\rho_{hv} < 0.96$ were not used in the analysis.

Although the described procedure for estimating the variability in the raindrop characteristic sizes at different scales was used for slanted observation geometry, it is assumed that the resulting estimates are representative for the horizontal variability. This assumption is based on the facts that the thickness of the rain layer in the observed wintertime events was relatively small and that the vertical variability in the radar measurements as estimated from range–height indicator scans was low (Matrosov et al. 2007). A more straightforward estimation of the horizontal variability in D_m could be performed if the constant-altitude PPI scans were available. The reconstruction of such scans, however, was not practical for the HMT-06 HYDROX radar operations, because the next elevation angle in volume scans was 4.5° and the radar observations at such an elevation in shallow precipitation were affected by regions of melting hydrometeors and snow at relatively short distances from the radar. At a 3° elevation beam, the range of heights sampled inside of the area of interest was about 0.5–1.8 km (at the beam center).

Figure 3 shows the results of estimations of the raindrop characteristic size variability δD_m as a function of the averaged value of the mass-weighted mean drop diameter $D_m^{(a)}$, calculated in the same resolution area as δD_m . The presented results were obtained for different spatial scales during the experimental event of 30–31 December 2005. A consistent stratiform rain of moderate intensity was observed for a period of more than 24 h during this event, which was the main priority case for the HMT-06 deployment. The smallest presented spatial scale of 4.5 km (Fig. 3c) approximately corresponds to the horizontal resolution of the TRMM spaceborne radar.

It can be seen from the Fig. 3 results that there is some general decrease of δD_m as $D_m^{(a)}$ increases. This decrease is more obvious for larger spatial scales. Overall, the characteristic size variability is greater for larger scales. The average values of δD_m [for data with $D_m^{(a)} > 1$ mm] in Fig. 3 are 0.33, 0.29, and 0.24 mm for resolutions of 20, 10, and 4.5 km, respectively. Data obtained with different positions of squares with smaller resolutions (i.e., with those whose sides are less than 20 km) inside the

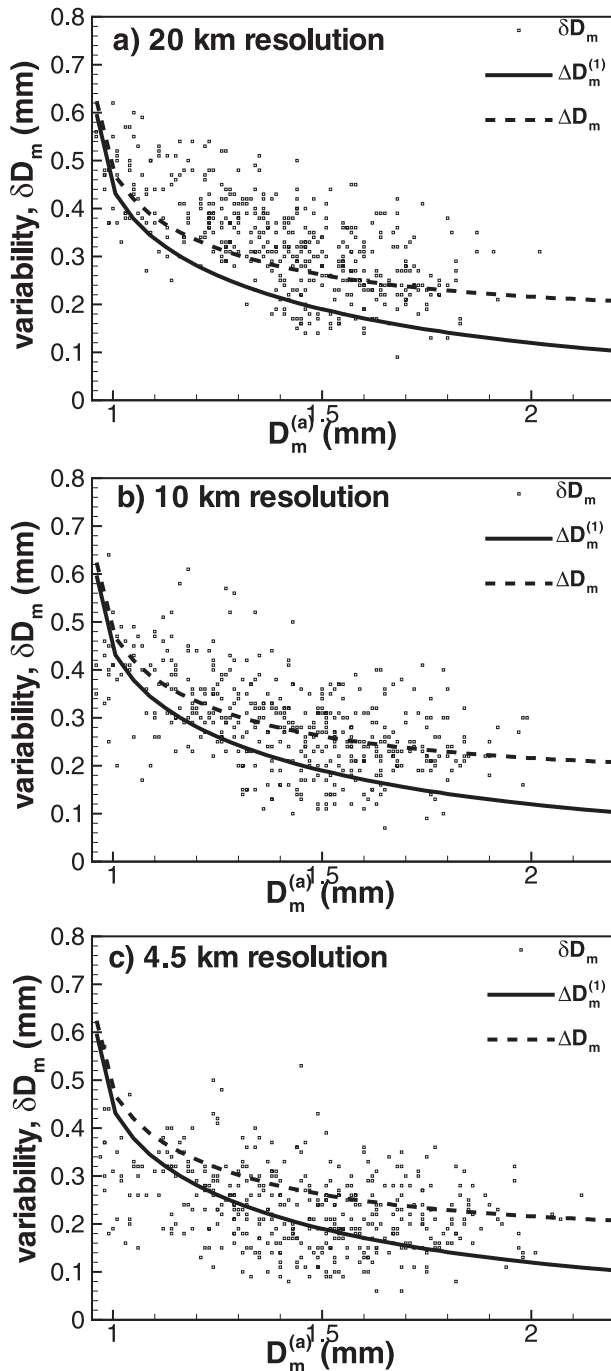


FIG. 3. Estimates of the absolute variability in mean mass-weighted drop sizes at spatial scales of (a) 20, (b) 10, and (c) 4.5 km as a function of the average of this size. Dashed lines depict possible total retrieval errors, and solid lines show those that are due to Z_{DR} measurement noise.

HYDROX coverage area showed that there is little dependence of variability estimates on these positions, and therefore the results of Fig. 3 are representative for general estimates of δD_m at different spatial scales.

b. Estimations of retrieval uncertainties

The drop size variability estimates need to be considered in the context of errors that are intrinsic to differential reflectivity-based retrievals. As mentioned in section 2, a value of 0.2 dB could be considered as a noise level in the gridded differential reflectivity data. The solid curves in Fig. 3 show D_m retrieval uncertainties $\Delta D_m^{(1)}$, which correspond to the 0.2-dB uncertainty in Z_{DR} ($\Delta Z_{DR} = 0.2$ dB) if Eq. (2) is used for retrievals. The uncertainties $\Delta D_m^{(1)}$ were calculated from

$$\Delta D_m^{(1)} = 0.5[1.8(Z_{DR} + 0.2)^{0.4} - 1.8(Z_{DR} - 0.2)^{0.4}], \quad (3)$$

where $Z_{DR} = [D_m^{(a)}/1.8]^{1.0/0.4}$.

The uncertainties $\Delta D_m^{(1)}$ decrease with Z_{DR} [and thus with $D_m^{(a)}$] because of the nonlinearity of the relation in Eq. (2). The data points that are located above these curves can be regarded as “reliable” at a given level of uncertainty (i.e., 1 standard deviation) in the absolute Z_{DR} values if a “perfect” 1-to-1 correspondence between D_m and Z_{DR} is assumed. The percentages of such points (as compared with the total datapoint number) corresponding to $\Delta Z_{DR} = 0.2$ dB and $D_m^{(a)} > 1$ mm in Fig. 3 are 90%, 78%, and 57% for the resolutions of 20, 10, and 4.5 km, respectively.

Uncertainty in Z_{DR} data is one source of drop size retrieval errors, but another error source is the variability of DSD shapes (as observed in HMT-06), which results in the data scatter around the mean D_m - Z_{DR} relation (i.e., the parameterization error). Equation (2) was derived for the HMT-06 DSDs. The standard deviation of data scatter in individual D_m values around this mean relation [$\Delta D_m^{(2)}$] is about 0.2 mm (Matrosov 2010), which corresponds to approximately 15% if expressed as a ratio of $\Delta D_m^{(2)}$ to the average for drop size observed during HMT-06. Assuming the independence of the error contributions due to the Z_{DR} data noise and due to DSD shape variations, the total retrieval error ΔD_m can be estimated from

$$\Delta D_m = \{[\Delta D_m^{(1)}]^2 + [\Delta D_m^{(2)}]^2\}^{0.5}. \quad (4)$$

The dashed curves in Fig. 3 show estimates of this error. For smaller raindrop mass-weighted sizes, the Z_{DR} data noise dominates the total retrieval error (i.e., the solid and dashed curves are very close). At larger characteristic drop sizes $D_m^{(a)}$, the data scatter around the mean D_m - Z_{DR} relation contributes noticeably to the total retrieval error. The relative contribution of the $\Delta D_m^{(2)}$ to the total uncertainty increases with the average drop size. The percentages of the individual data points that are above the dashed curves representing the total

retrieval error estimate ΔD_m are only about 74%, 54%, and 30% for the estimate resolutions of 20, 10, and 4.5 km, respectively.

The relative variability of drop mean mass-weighted diameters, which is expressed as the ratio $\delta D_m/D_m^{(a)}$, is shown in Fig. 4. A decreasing trend of the relative variability with an increase in the average characteristic size of raindrops is more pronounced relative to the trends in the absolute variability δD_m . This trend, however, diminishes as the horizontal scale at which the raindrop size variability is considered decreases. As in Fig. 3, Fig. 4 also shows the error-bound curves. The percentages of the individual data points that lie above these curves are the same as those cited for the Fig. 3 data.

4. Effects of the differential attenuation correction, polarization cross-talk, and mean drop shape-size assumption

X-band frequency signals experience noticeable attenuation in rain. Because the rate of this attenuation is different for horizontal and vertical polarization signals, the differential attenuation corrections must be introduced for differential reflectivity measurements. The customary way to correct for the effects of differential attenuation is by using a relation between the specific differential attenuation A_{DP} and specific differential phase shift on propagation K_{DP} , which is the range derivative of the differential phase on propagation. For the HMT-06 data the corresponding mean linearized relation was found:

$$A_{DP} \text{ (dB km}^{-1}\text{)} = 0.044K_{DP} \text{ (}^\circ\text{ km}^{-1}\text{)}. \quad (5)$$

This relation was used in correcting HYDROX differential reflectivity data using direct measurements of the total differential phase shift Φ_{DP} that were smoothed to minimize influences of the backscatter differential phase. The use of the linearized A_{DP} - K_{DP} relation is a certain simplification in the Z_{DR} correction scheme since some nonlinearity in this relation usually exists. Bringi and Chandrasekar (2001), for example, point out that at X band a value of the exponent in a power-law A_{DP} - K_{DP} relation could be about 1.15. The sensitivity of the characteristic drop size variability to Z_{DR} corrections is evaluated as part of this study.

Figure 5b shows a scatterplot of the range dependence of measured (i.e., noncorrected) values of differential reflectivity from HMT-06 HYDROX radar observations. These data correspond to backscatter from rain with $\rho_{hv} \geq 0.96$. The noncorrected values of Z_{DR} exhibit a noticeable decreasing trend with range. Given a large number of data points, this is an indication of a negative bias in measurements as a result of differential

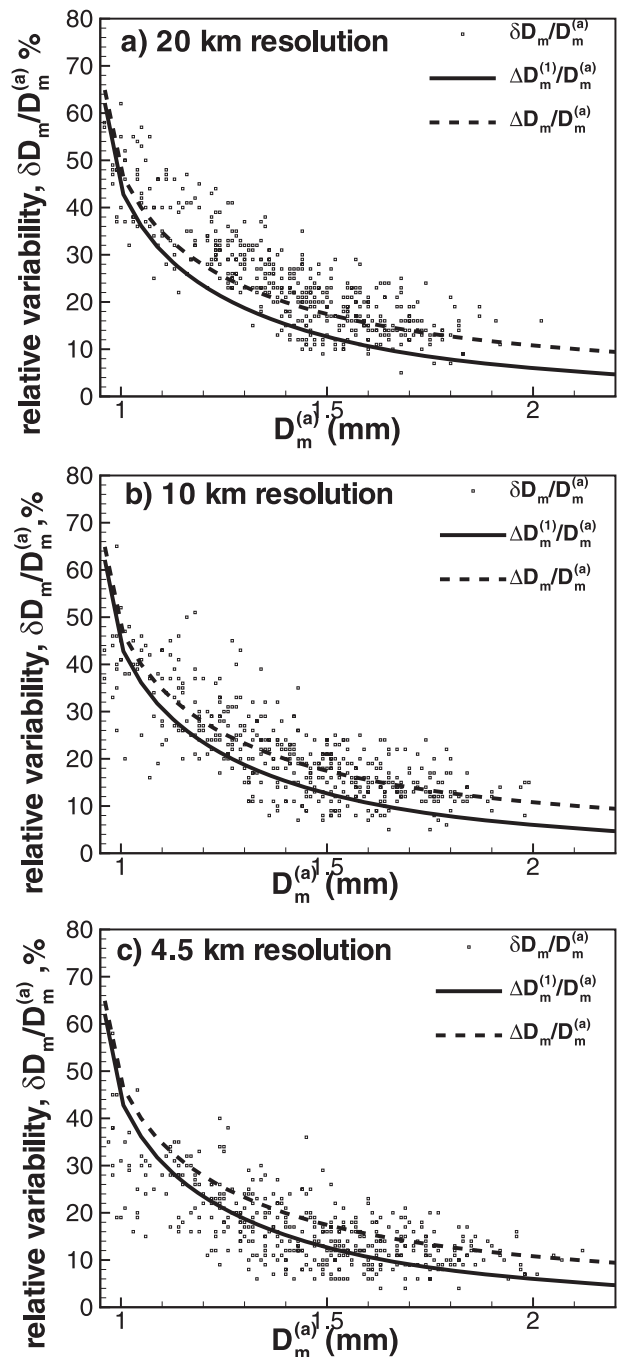


FIG. 4. As in Fig. 3 but for the relative variability in mean mass-weighted drop sizes. Dashed lines depict possible total relative retrieval errors, and solid lines depict those that are due to Z_{DR} measurement noise.

attenuation because, on average, the observed stratiform rainfalls were not becoming lighter with range, as estimated from gauges. Some increasing trend, however, is not out of the question because of the possible orographic effects that could increase rainfall at higher

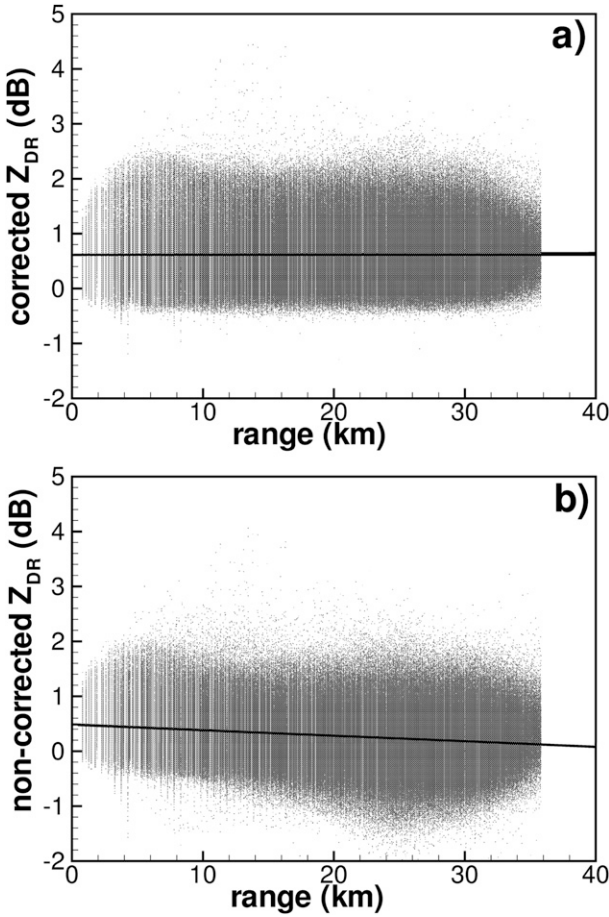


FIG. 5. Scatterplots of HYDROX differential reflectivity values vs range: (a) values corrected for differential attenuation effects using differential phase measurements and (b) values measured by the radar.

elevations observed at longer ranges. Terrain elevations in the HYDROX coverage area were changing generally within approximately 500 m. Unlike for noncorrected differential reflectivity, the corrected Z_{DR} (Fig. 5a) does not show any noticeable trend with range. The minimum values of corrected Z_{DR} are around -0.2 dB. They generally come from drizzle-like raindrops that are quasi-spherical and thus are expected to provide Z_{DR} of ~ 0 dB \pm noise. This is an independent indication of the noise level in the gridded differential reflectivity values that was estimated at 0.2 dB in section 2.

Another way to evaluate differential reflectivity data is to analyze Z_{DR} trends as a function of Φ_{DP} . It may be a more-robust evaluation because differential attenuation corrections are proportional to Φ_{DP} (under a simplified assumption of the A_{DP} - K_{DP} relation linearity). The backscatter phase-shift influence is expected to be small in stratiform rain with the relatively small drop sizes that were observed during the HMT-06.

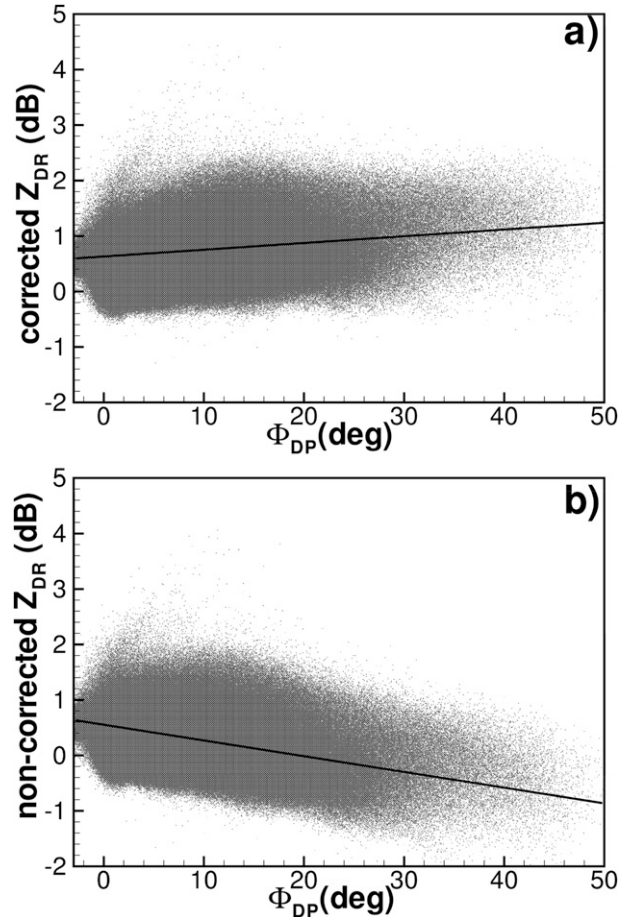


FIG. 6. As in Fig. 5 but vs differential phase.

Obvious manifestations of this phase shift were very rare in HYDROX measurements. The scatterplots of corrected and noncorrected HYDROX differential reflectivity values versus measured total differential phase are shown in Fig. 6. Note that the initial differential phase at the zero range $\Phi_{DP}(0)$ was set to zero as a result of tuning the radar hardware. The mean value of $\Phi_{DP}(0)$ was stable for the duration of the radar deployment. The standard deviation of the initial phase was estimated as about 3° .

The decreasing trend of noncorrected values of differential reflectivity with Φ_{DP} is obvious. For corrected Z_{DR} , there is a small increasing trend that is close to linear and can be approximated as

$$Z_{DR} \text{ (dB)} \approx 0.6 + 0.01\Phi_{DP} \text{ (}^\circ\text{)}. \quad (6)$$

There are several plausible explanations for the small gradual increase of corrected differential reflectivity with increasing differential phase. One explanation is that the Z_{DR} data were “overcorrected” on average because the coefficient in Eq. (5) was too large (e.g.,

because of the assumption for the mean drop shape–size relation). Other plausible explanations are uncertainties associated with the linear assumption between A_{DP} and K_{DP} and/or that orographic effects in the area of HYDROX measurements influenced rainfall so that there was some small increase in drop sizes with increasing differential phase shift.

One more factor that can be responsible for the differential-phase-shift-dependent bias in Z_{DR} measurements is antenna polarization cross coupling. This cross coupling can exist even for the mean vertical orientation of hydrometeors when polarimetric measurements are conducted in the STSR mode (Wang and Chandrasekar 2006; Hubbert et al. 2010). The Z_{DR} cross-coupling bias depends on the radar antenna linear depolarization ratio (LDR) limit. The estimated HYDROX radar system depolarization ratio limit was only from about -22 to -24 dB (Matrosov 2004). At such a limit, a differential reflectivity bias (in decibels) of about $0.01\Phi_{DP}$ (where Φ_{DP} is in degrees) could be expected according to the Fig. 12a data in Hubbert et al. (2010). Note that, according to the data presented in that figure, the cross-coupling bias depends on Φ_{DP} in a sine-curve manner when the transmitted polarization is 45° linear. For Φ_{DP} values that are less than about 40° (which was the case for the great majority of the HYDROX radar data obtained during the HMT-06 deployment as seen from Fig. 6), this bias dependence on the differential propagation phase shift can be considered to be approximately linear.

The factors mentioned above individually or in some combination could be a reason for the small positive trend of corrected Z_{DR} with Φ_{DP} in Fig. 6a. It is outside the scope of this study to establish the exact partitioning of the influences caused by these factors. The sensitivity of the estimates of the characteristic drop size variability to these factors, however, can be assessed in a relatively straightforward way.

Influences of different assumptions on characteristic drop size variability estimates

Figure 7a shows the variability of the drop mean mass-weighted diameter δD_m as a function of the average size $D_m^{(a)}$ at the largest-resolution 20-km scale. The data for this figure were calculated when the value of the coefficient in the linearized A_{DP} – K_{DP} relation in Eq. (5) was 0.034 instead of 0.044, which was used to obtain the results shown in section 3 (i.e., Figs. 3 and 4). The use of 0.034 instead of 0.044 eliminates the bias in corrected Z_{DR} as a function of Φ_{DP} that otherwise is present as seen in Fig. 6a. If the polarization cross-coupling effect has a dominant effect on the mean Z_{DR} change with Φ_{DP} , such tuning of this coefficient can be considered as

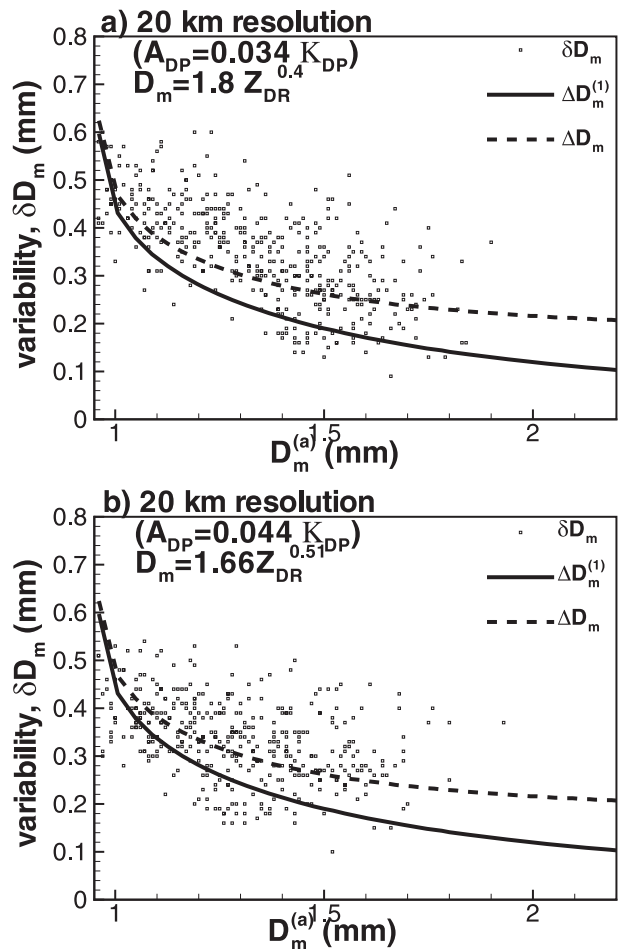


FIG. 7. Estimates of the absolute variability in mean mass-weighted drop sizes at spatial scales of 20 km for different A_{DP} – K_{DP} and D_m – Z_{DR} relations: (a) $A_{DP} = 0.034K_{DP}$ and $D_m = 1.8Z_{DR}^{0.4}$ and (b) $A_{DP} = 0.044K_{DP}$, $D_m = 1.66Z_{DR}^{0.51}$.

some kind of “balancing act” for minimizing this effect when total Φ_{DP} values are small enough (e.g., $<40^\circ$) that Z_{DR} cross-coupling bias– Φ_{DP} dependences are quasi linear.

Figure 7b shows the results of estimates of drop characteristic size variability at the 20-km scale if the relation D_m (mm) = $1.66Z_{DR}^{0.51}$ (dB) [rather than Eq. (2)] was used for estimating drop characteristic size. This relation was obtained using a drop shape–size model that linearly approximates drop oblateness (for $D > 0.5$ mm) as a function of drop diameter (Matrosov 2010) as opposed to the polynomial function used for deriving Eq. (2). Note that the choice of the drop shape model affects relative changes in drop sizes to a smaller extent than it does the absolute values of these sizes.

A comparison of Figs. 7a and 7b with Fig. 3a reveals that the described changes in the differential attenuation correction coefficient and in the D_m – Z_{DR} relation influence results for the spatial scale of 20 km in a

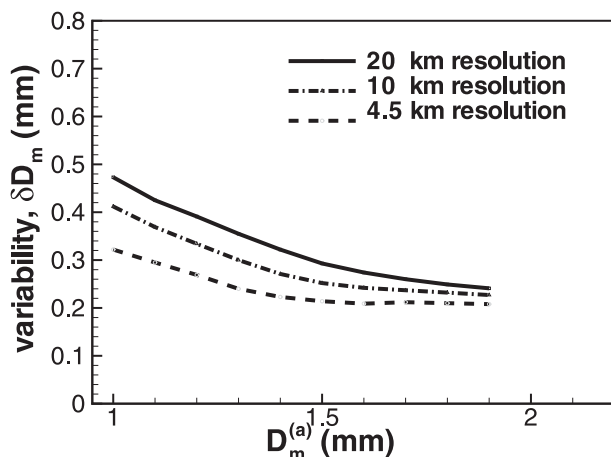


FIG. 8. Mean values of the drop size variability as a function of the average drop size for different resolutions.

relatively modest way. The mean values of δD_m are 0.325, 0.341, and 0.332 mm for the data in Figs. 3a, 7a, and 7b, respectively. The number of data points above the error lines in these figures varies only within a few percentage points. The differences between the results for the smaller spatial scales are even less significant than those shown for the 20-km scale, and thus they are not depicted.

5. Mean trends in drop size variability

The section-3 examples of estimating the variability of the mean mass-weighted drop diameter D_m at different spatial scales were shown for the priority event from the HYDROX radar HMT-06 field observations. These event data are representative for the whole dataset collected during 2005/06. Figure 8 shows the variability δD_m obtained using the whole dataset as a function of the average size $D_m^{(a)}$ at different spatial scales. The curves in this figure represent the mean values of δD_m . The corresponding relative standard deviations are typically between 20% and 30% (not shown).

To assess the influence of the choice of the area in which drop size variability assessments were performed, estimations of δD_m were also conducted for different 20-, 10-, and 4.5-km areas randomly fitted within the radar coverage region. The results indicated that there was relatively little change in δD_m estimates when these areas varied but the spatial scale was preserved. In general, δD_m values obtained for different locations of the estimation areas differed by not more than 5%–7% from those shown in Fig. 8. Because the mean terrain elevations varied for different drop size variability estimation areas, these results also indicate that the probable influence of orographic effects on the δD_m values obtained in this study was relatively minor.

There is a decreasing trend for δD_m when the average drop size increases. Mean δD_m values decrease by about 1.7, 1.5, and 1.4 when average mass-weighted drop sizes increase from 1 to 2 mm for spatial resolutions of 20, 10, and 4.5 km, respectively. For a given average drop size $D_m^{(a)}$, the drop size variability δD_m is greater for larger resolutions. The differences in the variability at different resolutions diminish with $D_m^{(a)}$. It should be mentioned, however, that estimates of the variability parameter δD_m from differential reflectivity measurements are more reliable for greater resolutions. For resolutions that are greater than about 10 km, usually more than 50% of the individual estimates of δD_m are greater than the uncertainty caused by the measurement errors and the retrieval-method errors. As resolution decreases, the fraction of data points producing variability estimates, which are noisy, increases. This is a limitation of the differential reflectivity–based approach for estimating characteristic raindrop sizes.

This limitation precludes robust estimations of the characteristic drop size resolution at smaller spatial scales (even though the corresponding results may look consistent), at least in rainfall observed during HMT. This rainfall was predominantly stratiform, and the dynamic range in mean values of D_m was not very large. According to disdrometer data collected in the ARB during different years (Matrosov 2010), values of D_m very rarely exceeded 2 mm.

6. Discussion and conclusions

Differential reflectivity measurements from a scanning polarimetric X-band radar were examined for the purpose of retrieving raindrop mean mass-weighted diameters D_m and estimating D_m variability at different spatial scales. Measurements were performed in wintertime shallow stratiform rainfall using the NOAA HYDROX X-band scanning polarimetric radar, which was deployed as part of the 2005/06 HMT field project in the American River basin. The radar measurements of Z_{DR} were calibrated using the vertical beam incidence observations and were corrected for the effects of differential attenuation using differential phase-shift data. For the considered dataset, the values of D_m and Z_{DR} were typically less than about 2.5 mm and 2 dB, respectively. The measurement noise of gridded Z_{DR} data was estimated as 0.2 dB. The D_m retrieval errors precluded reliable retrievals of mean D_m values, which were less than about 0.9–1 mm. This is considered to be a common limitation for polarimetric radar–based approaches for DSD parameter retrievals.

The examination of the characteristic drop size retrieval results revealed their greater variability for larger

spatial scales. Mean values of this variability δD_m , which are defined as the standard deviations of D_m at different horizontal scales, were found to be around 0.32–0.34, 0.28–0.30, and 0.24–0.26 mm at the scales of 20, 10, and 4.5 km, respectively. These estimates showed little sensitivity to the location of the area where estimations were performed, which indicates that the possible influence of orographic effects was not significant for the dataset considered in this study.

For a given spatial scale, there is a decreasing trend of δD_m when the mean value of the drop mean mass-weighted diameter increases. For a 20-km scale, this trend results in a decrease of δD_m by about a factor of 1.7 when the average value of D_m increases from 1 to 2 mm. Estimation data suggest that the trend of diminishing drop size variability with increasing average drop size becomes less pronounced for smaller spatial scales. For scales of 10 and 4.5 km, values of δD_m decrease only by a factor of about 1.5 and 1.4, correspondingly. A diminishing trend of δD_m with an increase in D_m results from differences in microphysical and kinematic processes providing different characteristic drop sizes and their variability (i.e., the physically based influence) and also from the general decrease of the retrieval error with increasing D_m . It is difficult to decouple these two influences, although the presence of the physically based influence can be seen from the fact that the diminishing trend of δD_m with increasing D_m is more pronounced at larger spatial scales (e.g., ~ 20 km) where ratios of size variability to retrieval error are greater than at smaller spatial scales (e.g., as seen from Figs. 3 and 4).

The measurement noise in Z_{DR} data and the data scatter in the D_m – Z_{DR} relation used for retrievals, resulted in only about 74%–84%, 52%–66%, and 30%–37% of all individual δD_m data points being above the estimated uncertainties of the retrievals for the scales of 20, 10, and 4.5 km, respectively. The spread in the above percentage points is due to the different D_m – Z_{DR} relations and different coefficients in the differential attenuation correction schemes that were applied. The use of different D_m – Z_{DR} relations and different coefficients for Z_{DR} corrections was part of evaluating the sensitivity of the results to various assumptions.

The influences of possible polarization cross coupling due to the antenna LDR limitation were evaluated as part of tuning the coefficient in the differential attenuation–differential phase shift relation. It was suggested that if total Φ_{DP} values in the rain media are less than about 40° and $\Phi_{DP}(0) = 0^\circ$, tuning of this coefficient can balance off a possible Z_{DR} polarization cross-coupling bias because both the differential attenuation correction and this bias depend on Φ_{DP} in an approximately linear way. It should be admitted,

however, that cross coupling is just one of the possible reasons for the original overcorrection of Z_{DR} values. Uncertainties due to “linearization” of A_{DP} – K_{DP} relations and some orographic effects resulting in gradual drop size changes can also play a role. More studies are needed to understand better the effects of polarization cross coupling with the radars employing the simultaneous transmission–simultaneous receiving measurement mode.

The average tendency of the diminishing drop size variability as the spatial scale, at which this variability is estimated, decreases is evident. However, the fact that often a significant number of the δD_m estimates for spatial scales, which are less than about 10 km, are smaller than possible uncertainties of D_m estimates from radar data points to a certain limitation of the polarimetric radar–based assessment of the variability in characteristic drop sizes at such scales. Although the drop characteristic size variability estimates at smaller scales appear to be consistent with the results obtained for larger scales and the observed tendencies with decreasing scale size are expected, the results for these smaller scales generally cannot be considered to be very robust. This finding is believed to be a common limitation of polarimetric radar–based approaches for inferring characteristic raindrop sizes from differential reflectivity data, which have a typical measurement uncertainty on the order of 0.2 dB. This limitation and a general noisiness of Z_{DR} measurement data also precluded estimates of other characteristics of the drop size spatial variability such as decorrelation lengths and spatial structure functions that generally require accurate estimates of analyzed parameters at fine spatial scales.

Rainfall observed during the HMT-06 HYDROX radar deployment was mostly of the stratiform type with a clearly defined radar bright band caused by melting snowflakes. Rainfalls with convective features are likely to exhibit greater variability in DSD properties, including the characteristic drop size. The polarimetric radar approaches applied for such rainfalls may be more helpful for estimating parameters of drop size variability parameters at smaller spatial scales, because the ratio of drop size variability to the drop size retrieval uncertainty will be greater than it is for the events observed during HMT-06.

Acknowledgments. This research was funded through the NOAA HMT Project and Grant NA17RJ1229.

REFERENCES

- Barber, P., and C. Yeh, 1975: Scattering of electromagnetic waves by arbitrarily shaped dielectric bodies. *Appl. Opt.*, **14**, 2864–2872.

- Brandes, E. A., G. Zhang, and J. Vivekanandan, 2005: Corrigendum. *J. Appl. Meteor.*, **44**, 186.
- Beard, K. V., and C. Chuang, 1987: A new model for the equilibrium shape of raindrops. *J. Atmos. Sci.*, **44**, 1509–1524.
- Bringi, V. N., and V. Chandrasekar, 2001: *Polarimetric Doppler Weather Radar*. Cambridge University Press, 636 pp.
- Chandrasekar, V., A. Hou, E. Smith, V. N. Bringi, S. A. Rutledge, E. Gorgucci, W. A. Petersen, and G. Skofronick Jackson, 2008: Potential role of dual-polarization radar in the validation of satellite precipitation measurements: Rationale and opportunities. *Bull. Amer. Meteor. Soc.*, **89**, 1127–1145.
- Doviak, R. J., V. Bringi, A. Ryzhkov, A. Zahrai, and D. Zrnica, 2000: Considerations for polarimetric upgrades to operational WSR-88D radars. *J. Atmos. Oceanic Technol.*, **17**, 257–278.
- Huang, G. J., V. N. Bringi, and M. Thurai, 2008: Orientation angle distribution of drops after an 80-m fall using a 2D video disdrometer. *J. Atmos. Oceanic Technol.*, **25**, 1717–1723.
- Hubbert, J. C., S. M. Ellis, M. Dixon, and G. Meymaris, 2010: Modeling, error analysis, and evaluation of dual-polarization variables obtained from simultaneous horizontal and vertical polarization transmit radar. Part I: Modeling and antenna errors. *J. Atmos. Oceanic Technol.*, **27**, 1583–1598.
- Matrosov, S. Y., 2004: Depolarization estimates from linear H and V measurements with weather radars operating in simultaneous transmission–simultaneous receiving mode. *J. Atmos. Oceanic Technol.*, **21**, 574–583.
- , 2010: Evaluating polarimetric X-band radar rainfall estimators during HMT. *J. Atmos. Oceanic Technol.*, **27**, 122–134.
- , D. E. Kingsmill, B. E. Martner, and F. M. Ralph, 2005: The utility of X-band polarimetric radar for quantitative estimates of rainfall parameters. *J. Hydrometeorol.*, **6**, 248–262.
- , R. Cifelli, P. C. Kennedy, S. W. Nesbitt, S. A. Rutledge, V. N. Bringi, and B. E. Martner, 2006: A comparative study of rainfall retrievals based on specific differential phase shifts at X- and S-band radar frequencies. *J. Atmos. Oceanic Technol.*, **23**, 952–963.
- , C. A. Clark, and D. A. Kingsmill, 2007: A polarimetric radar approach to identify rain, melting-layer, and snow regions for applying corrections to vertical profiles of reflectivity. *J. Appl. Meteor. Climatol.*, **46**, 154–166.
- Seliga, T. A., and V. N. Bringi, 1976: Potential use of radar differential reflectivity measurements at orthogonal polarizations for measuring precipitation. *J. Appl. Meteor.*, **15**, 69–76.
- Sheppard, B. E., and P. I. Joe, 1994: Comparison of raindrop size distribution measurements by a Joss–Waldvogel disdrometer, a PMS 2DG spectrometer, and a POSS Doppler radar. *J. Atmos. Oceanic Technol.*, **11**, 874–887.
- Thurai, M., M. Szakall, V. N. Bringi, K. V. Beard, S. K. Mitra, and S. Borrmann, 2009: Drop shapes and axis ratio distributions: Comparisons between 2D video disdrometer and wind tunnel measurements. *J. Atmos. Oceanic Technol.*, **26**, 1427–1432.
- Ulbrich, C. W., 1983: Natural variations in the analytical form of the raindrop size distribution. *J. Climate Appl. Meteor.*, **22**, 1764–1775.
- Wang, Y., and V. Chandrasekar, 2006: Polarization isolation requirements for linear dual-polarization weather radar in simultaneous transmission mode of operation. *IEEE Trans. Geosci. Remote Sens.*, **44**, 2019–2028.
- Willis, P. T., 1984: Functional fits to some observed drop size distributions and parameterizations of rain. *J. Atmos. Sci.*, **41**, 1648–1661.
- Zhang, G., J. Vivekanandan, E. A. Brandes, R. Meneghini, and T. Kozu, 2003: The shape–slope relation in observed gamma raindrop size distributions: Statistical error or useful information? *J. Atmos. Oceanic Technol.*, **20**, 1106–1119.